

Diffusion mechanism of bound Schottky defect in magnesium oxide

Sami Mahmoud^{1,*}, Philippe Carrez¹, Marie Landeiro Dos Reis¹, Normand Mousseau² and Patrick Cordier^{1,3}

¹Université de Lille, CNRS, INRAE, Centrale Lille, UMR 8207 - UMET - Unité Matériaux et Transformations, F-59000 Lille, France

²Département de physique and Regroupement québécois sur les matériaux de pointe, Université de Montréal, CP 6128, Succursale Centre-Ville, Montréal, Québec H3C 3J7, Canada

³Institut Universitaire de France, 1 rue Descartes, F-75005 Paris, France



(Received 21 September 2020; accepted 12 March 2021; published 25 March 2021)

In simple ionic crystals, intrinsic point defects must satisfy electrical neutrality and exist as Schottky defects. In magnesium oxide (MgO), a Schottky defect is then a combination of anionic and cationic vacancies. Since vacancies are charged, the stable configuration of the Schottky defect corresponds to a bound pair of vacancies of opposite signs. In this study, we investigate the kinetics of formation and migration of such a bound pair on long timescales reaching in some cases thousands of seconds using the kinetic activation-relaxation technique, an off-lattice kinetic Monte Carlo method with an event catalog built on-the-fly during static molecular simulations. We show that the diffusion of this bound Schottky defect involves the migration of vacancies bounded to the first and third neighbor sites of the crystal structure with an apparent migration energy which cannot be inferred from the migration energies expected from isolated defects. Overall, this study gives insights and constraints on the oxygen diffusion mechanism reported experimentally in high-purity MgO samples.

DOI: [10.1103/PhysRevMaterials.5.033609](https://doi.org/10.1103/PhysRevMaterials.5.033609)

I. INTRODUCTION

In ionic crystals, a Schottky defect (SD) is a combination of point defects which satisfies electrical neutrality. Since the presence and the diffusion of point defects, including Schottky defects, in ionic crystals can affect directly the mechanical, chemical, and even optical properties of materials, the point defect chemistry and point defect diffusion properties in ionic materials have been the subjects of numerous studies [1–3]. A comprehensive overview of diffusion properties includes theoretical studies with the aim to provide not only formation energies of point defects but also activation energies for diffusion. Nevertheless, a comprehensive treatment of point defect properties remains challenging from the experimental point of view but also on the theoretical side. An example is complex point crystal chemistry in ionic materials which may lead to experimental restrictions in the determination of concentrations and diffusion coefficient of intrinsic species. Numerically, standard *ab initio* and classical molecular dynamics (MD) methods suffer from spatiotemporal limitations that often prevent them from accessing scales relevant to experimental conditions. Over the last decades, however, new algorithms have made it possible to lift these limitations while preserving the richness of the energy landscape. This is the case of the kinetic activation-relaxation technique (kART), a fully off-lattice kinetic Monte Carlo (KMC) method with on-the-fly construction of the event catalog [4–7]. This method lifts the traditional constraints of standard KMC approaches, which require beforehand knowledge of the activation events and include only limited treatment of the short- and long-range important elastic effects. Magnesium oxide (MgO) in

its rocksalt structure (B1) has been considered for many years as an archetype material for the physical characterization of ionic solids and ceramics. It has also long been considered as a reference material for both experiments and theories to probe growth mechanisms in charge transfer taking place in insulating oxides [8,9]. In MgO, a Schottky defect is constituted by a pair of an oxygen and a magnesium vacancy. In this simple ionic structure, it is well established that oxygen diffusion is significantly slower than magnesium diffusion at least when point defects are considered individually. Indeed, because oxygen and magnesium vacancies are charged defects, the SD can exist as different configurations ranging from the isolated charged vacancies to a bound state. The diffusion of bound SDs has been discussed in MgO by Yang and Flynn [10] with respect to diffusion measurement of high-purity MgO grown by molecular beam epitaxy. However, the detailed mechanism for bound MgO vacancy pair diffusion is still unknown. Despite numerous theoretical studies, relying on both classical MD [11,12] and *ab initio* methods [13,14], involving accelerated MD [15], a proper description of bound SD migration is missing as recognized by Amman *et al.* [16] a few years ago. The limitations of standard methods as described above may explain why up to now, most of the diffusion studies have been focused on the diffusion paths of isolated vacancies [13,17]. The goal of this study is to fill the gap and to be able to constrain the oxygen vacancy diffusion mechanism in high-purity MgO as the one reported by Yang and Flynn [10]. We focus on the diffusion mechanism of a bound SD. Using the kART method, the kinetics of the various vacancy configurations are investigated over a large range of temperature and timescale. We establish the diffusion path of the SD in MgO and its temperature dependency by the determination of the diffusion coefficients.

*sami.mahmoud@univ-lille.fr

II. METHODS

A. Atomistic simulations

Throughout this study, molecular static simulations are performed using the LAMMPS (Large-scale Atomic/Molecular Massively Parallel Simulator) [18] code. The interactions between ions are modeled according to a classical pairwise potential of Buckingham form. Long-range interactions are thus relying on a Coulomb term here summed by means of the particle-particle-particle mesh (pppm) method [19] and at short range, the interaction Mg-O and O-O are explicitly treated by the Buckingham formulation. The parametrization used here corresponds to the Ball and Grimes model as described in Ref. [20], in which the charge of ions, q , is set to $\pm 1.7e$. Such a parametrization with partial charges is chosen for consistency with Bader charge analysis as determined from *ab initio* calculations [13] and was previously successfully applied to diffusion in MgO [20]. In the following, atomistic simulations are performed with 3D periodic boundary conditions for system sizes ranging from 2744 atoms to 195 112 atoms and energy minimization is achieved by means of a fast inertial relaxation engine (FIRE) algorithm [21]. According to the potential parametrization, the lattice parameter a of MgO is equal to 4.2182 Å, which is consistent with its experimental determination [22,23].

B. Kinetic activation relaxation technique

Diffusion pathways for the SD vacancies are generated using the kinetic activation-relaxation technique (kART) [4,24]. For a complete overview of the ART method, one can refer to the recent reviews from Mousseau and co-workers [5,25]. In the next section, we briefly review the basic algorithm and specific parameters used in this study.

All kART simulations start from an initial configuration from which a pair of opposite vacancies have been randomly introduced. After a first minimization of the total configuration, an event catalog is generated. First, going through all atoms in the lattice, local topologies surrounding all atoms are determined using the graph isomorphism algorithm NAUTY [26]. A graph is generated by linking atoms contained in a sphere with a radius of 6 Å around the central atom according to a cutoff distance of 2.8 Å to ensure the inclusion of the first-neighbors atoms only. Self-loops are added to the second species to preserve chemical identity in the graphs. The generated graph, which contains about 80 summits, is then treated with NAUTY, which assigns a unique key to each different automorphic class and returns a map associating the summits of the specific graph with that of a generic one, facilitating the reconstruction of events. If the found topologies are not already in the catalog, a mapping of the events around the central atom is launched using the activation-relaxation technique (version ART nouveau or ARTn) [27,28]. This method offers a highly efficient and unbiased approach to find local transition states surrounding a given minimum, without the need to first guess a pathway [29]. For simple systems, 25 ARTn event searches are typically performed for each new topology; this number can be increased to 50 to ensure the completeness of the event catalog in more complex situations. The number of searches is also generally increased for frequent topologies. To ensure

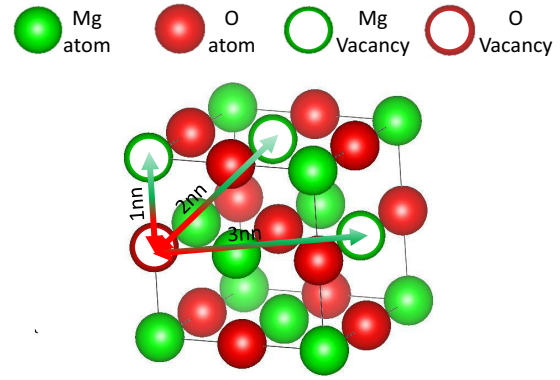


FIG. 1. View of the MgO unit cell showing the first, second, and third nearest neighbor distances separating the cationic and anionic vacancies, labeled 1nn, 2nn, and 3nn, respectively.

detailed balance, the connectivity between two states involved in the event is checked by relaxing from their saddle point in both directions and the event is added to the catalog associated with both the initial and final topologies. The transition state theory [30] is then applied when all events are well identified and the system evolves in time according to Poisson distribution law [31]. One event is chosen from the generated tree randomly which has a probability relative to its rate and thus the system advances from a step to another. To prevent being trapped by low-barrier events associated with nondiffusive mechanisms, we use the basin accelerated mean-rate method (bacMRM) [24] which solves them analytically. We choose a threshold of 0.1 eV to not consider these flickering states without affecting the real kinetic. To reduce computational costs, we also concentrate the searches for events only on atoms that are in noncrystalline environments, i.e., those that are within 4.0 Å from a defect. This restriction only removes the very high energy and events associated with the creation of a defect pair in the crystal, without affecting the kinetics of defects already present in the lattice.

C. Nudged elastic band calculations

In order to confirm the accuracy of the heights of some migration barriers found with kART, we used the climbing nudged elastic band (NEB) method [32,33]. It is a simulation technique that allows us to find the minimum energy path (MEP) between two predetermined relaxed states. The details of this method can be found in Ref. [32]. It is however important to make precise all the parameters that we used in our simulations. The force criterion was fixed to 1×10^{-6} eV/Å. We used 12 intermediate states and a relatively high spring constant ($2 \text{ eV}/\text{Å}^2$) to prevent intermediate replica to minimize the stable configuration and a time step of 0.1 fs.

III. RESULTS

A. Formation energy of Schottky defects

The formation energy of the SD was computed for different configurations (Fig. 1), corresponding to different distances d [involving different nearest neighbor (nn) shells] between vacancies of opposite types carrying opposite charges $\pm q$.

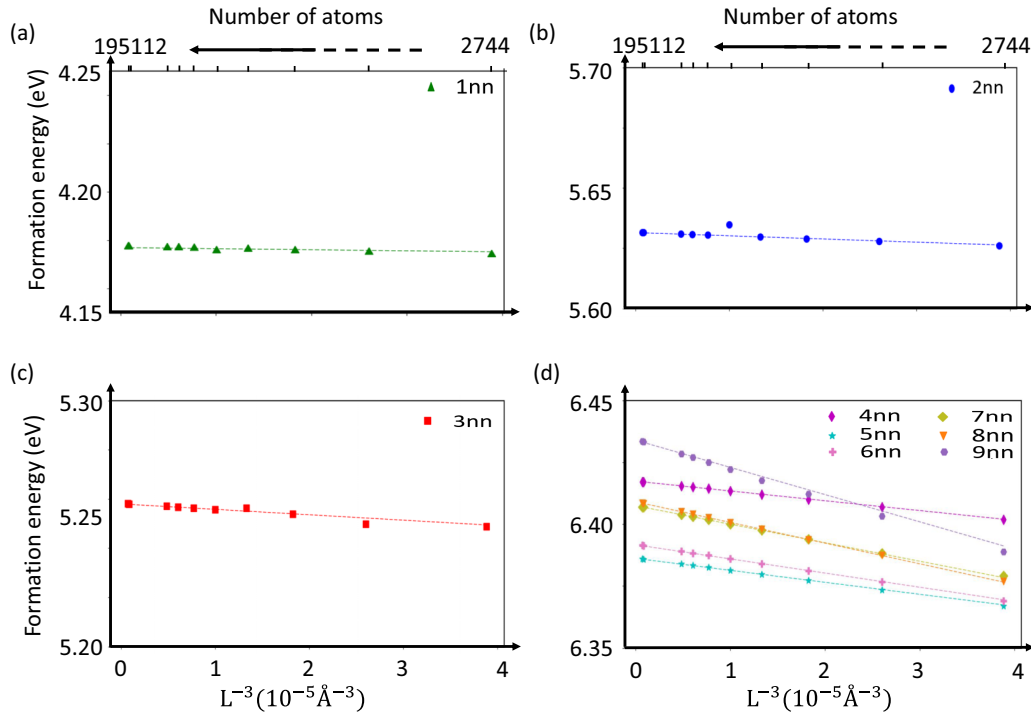


FIG. 2. Formation energy of Schottky defects for (a) 1nn, (b) 2nn, (c) 3nn, and (d) 4nn to 9nn configurations depending on cubic box volume L^3 and its corresponding number of atoms. Corrections and scaling (explained in Sec. III A) are indicated with dashed lines.

Since a pair of charged vacancies is introduced inside a periodic system of typical length L , in order to compute the SD formation energy E_F , one has to correct the minimized energy E_{SD} of the system for the long-range periodic interactions. Here the formation energy was evaluated from the following expression:

$$E_F = E_{SD} - NE_0 - E_{el}, \quad (1)$$

where E_{SD} is the energy of a system containing $2N$ ions and a SD, E_0 is the absolute energy of a pair of a magnesium and an oxygen ions in a bulk system, and E_{el} is the long-range periodic correction energy hereafter assumed to be in the form of an infinite dipole correction term and therefore scaling as a function of $\frac{d^2}{L^3}$. The effect of such correction can be observed in Fig. 2, and the corresponding SD formation energies are given in Table I.

The formation energies of the SD are configuration dependent; i.e., they depend on the distance d between the two vacancies of opposite charge (Fig. 2). The lowest formation energy, which defines the bound SD configuration, corresponds to the typical case of a divacancy where the vacancies are in the first nearest neighbor configuration (1nn) with $E_F = 4.18$ eV. When plotting the formation energies as a function of d as done in Fig. 3, it is seen that for widely spaced SDs, E_F follow a linear trend described by the Coulombic interaction between the two opposite charged defects. This trend tends, for infinitely spaced vacancies, to the value of 6.42 eV, a formation energy in excellent agreement with the one obtained from the independent calculations of the individual oxygen vacancy (V_O) and magnesium vacancy (V_{Mg}) formation energies (predicting 6.42 eV in the case of isolated (noninteracting) defects; the formation energy of isolated

vacancies has been calculated by introducing each vacancy inside the periodic system according to Leslie and Gillan's work [36]). At small spacing distance, we note that such a purely electrostatic (or Coulombic) behavior is not satisfied, suggesting that other contributions, including potentially an elastic relaxation of ions, also play a significant role in the energy budget. Consequently, the 3nn configuration has a formation energy lower than the 2nn configuration.

B. Kinetics of migration

The kART simulations are launched from an initial atomic configuration where the two vacancies are far from each other and run until defect aggregation is completed, typically over

TABLE I. Calculated Schottky defect formation energies at different configurations depending on distances separating the vacancies. The values are compared to available DFT results. All values are in eV.

Configuration	This work	DFT works
1nn	4.18	3.70 [34], 3.74 [34], 3.88 [16], 4.6 [13]
2nn	5.63	5.9 [13]
3nn	5.26	5.7 [13]
4nn	6.42	
5nn	6.39	
6nn	6.40	
7nn	6.40	
8nn	6.41	
9nn	6.44	
∞	6.42	5.54 [34], 5.79 [34], 5.97 [13], 6.88 [14], 7.5 [35]

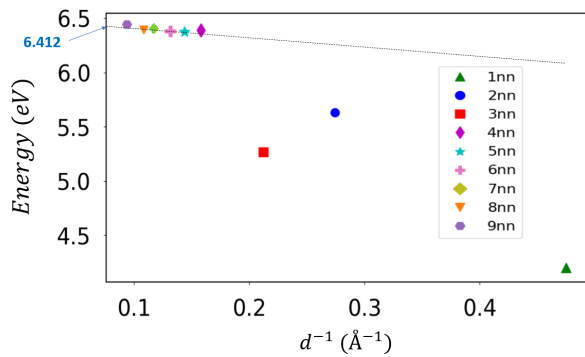


FIG. 3. Scaling of the SD formation energy with a Coulombic term, $\frac{q^2}{4\pi\epsilon d}$. ϵ is taken here as $8.5\epsilon_0$ as given by our parametrization of the interaction force field.

100 KMC steps or more. Simulations are repeated at various temperatures between 500 and 2000 K to establish the different diffusion modes for the SD. The mean squared displacements (MSDs) recorded during our set of simulations are shown in Fig. 4. Two different regimes can be distinguished in the MSD plots. A first, short, initially high-slope regime is followed by a second regime with a lower slope. The high-slope initial stage corresponds to the setup of the simulation, in which the two vacancies evolve initially from their almost isolated configuration to a 1nn bound SD configuration (i.e.,

the minimum energy configuration of the system). The second regime corresponds then to the motion of strongly correlated vacancies, i.e., the bound SD.

For both regimes, the slopes of the MSD are temperature dependent. In the first regime, depending on the temperature, the diffusion processes leading to the aggregation of defects involve the diffusion of the two vacancies at different rates. At low temperature, below about 1200 K, this transient regime is completely dominated by the cationic vacancy displacements with few or no V_O jumps. In this temperature range, V_O diffusion is negligible compared to V_{Mg} diffusion, and one may literally see V_{Mg} diffusing toward V_O in our simulations. At higher temperatures, both vacancies diffuse toward a 1nn SD configuration although one can still observe from Fig. 4 that V_{Mg} diffusion is faster than V_O .

Once vacancies are aggregated to form the 1nn SD, diffusion of the SD is conditioned by the anionic jumps as described kinetically later by describing the energy barriers of the dominant mechanisms.

C. Migration energies

When the vacancies are well separated (i.e., in the initial phase of the simulation), the migration energy barriers of Mg and O vacancies are 1.53 eV and 1.70 eV, respectively. Since our calculations show that once the vacancies aggregate into a divacancy (1nn configuration) the bound SD exhibits a distinct

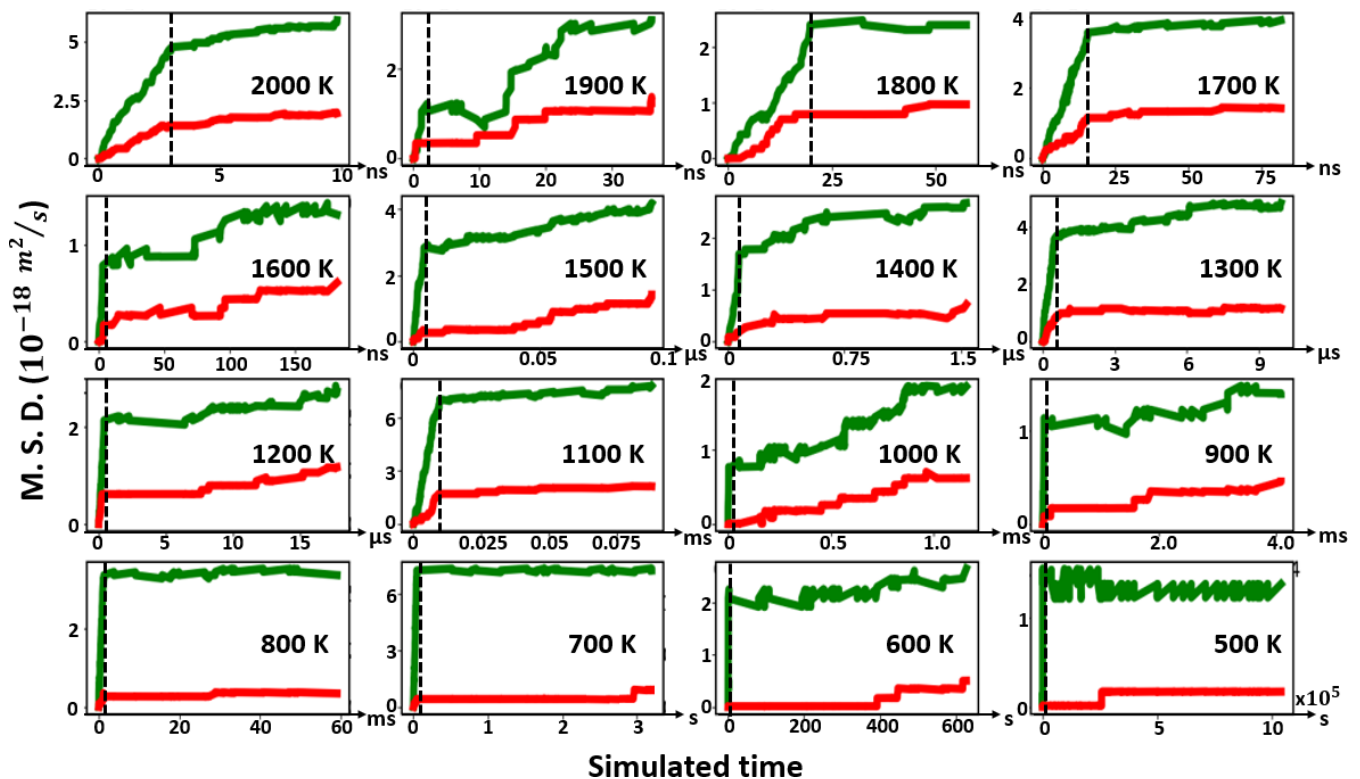


FIG. 4. Mean squared displacement (MSD) as a function of the elapsed time of cationic and anionic vacancies in MgO. Green and red tracers are relative to Mg and O vacancies respectively. 16 graphs are plotted at different temperatures in the range of 500–2000 K (indicated in each subplot) with steps of 100 K. The vertical discontinued lines indicate the dominant change in the diffusion slope. The diffusion coefficient is then calculated from the slopes of the MSD using $\frac{\langle D^2 \rangle}{6t}$ where $\langle D^2 \rangle$ is the mean squared displacement.

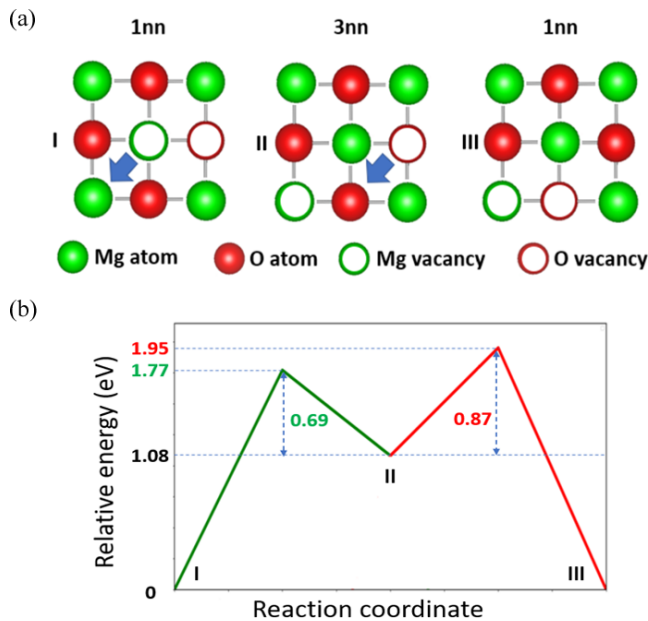


FIG. 5. (a) Cartoon and (b) energetic descriptions of the easiest diffusion path of Schottky defects. In (a) green and red circles represents Mg and O atoms, respectively, while empty circles refer to vacancies. In (b), green and red lines refer to Mg and O vacancy energetic evolution, respectively. The three indexes (I, II, and III) are used to identify states and explain the diffusion mechanism.

behavior, we have studied in more detail the dynamics of vacancies around this low-energy configuration. In our kART simulations, we observe that the 1nn configuration always dissociates by the jump of the Mg vacancy to form a 3nn SD [I to II in Fig. 5(a)]. The corresponding energy barrier is 1.77 eV. Most of the time, this cationic jump is followed by the reverse event (II to I) with a barrier of 0.69 eV which makes the V_{Mg} oscillating between 1nn and 3nn sites with no net displacement. However, starting from a 3nn configuration, as shown in Fig. 5(a), the anionic vacancy can jump to an atomic site corresponding to another 1nn configuration (II to III). The energy barrier corresponding to this event is 0.87 eV. Between I and III, the center of mass of the vacancy pair has moved which corresponds to a displacement of the divacancy.

As also reported in a recent work [37], the energy barriers of vacancy migration found by kART have been well reproduced by the NEB method in our study. First we have calculated the energy barriers corresponding to a Mg vacancy approaching an O vacancy starting from a far configuration [Fig. 6(a)]. The symmetric configuration (an O vacancy approaching a Mg vacancy) is shown in Fig. 6(b). One can clearly see how the system is evolving toward more stable configurations until the lower configuration energy is reached. The values of energy barriers found by ARTn are recovered by NEB calculations. We have also investigated in detail the possible jumps in the vicinity of the 1nn divacancy configuration. The corresponding energy paths are shown in Fig. 7. For both defects, the direct transition between two 1nn configurations involves the highest migration energy barriers, the one involving a V_O jump (2.96 eV) being even less favorable than the one involving a V_{Mg} jump (2.79 eV). Oppositely, we find

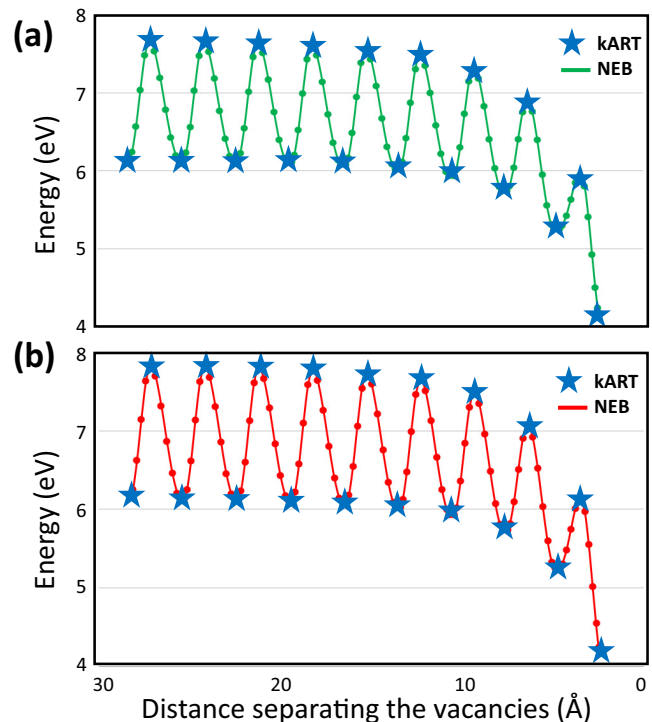


FIG. 6. Formation energy evolution using kART and NEB calculations, depending on distance separating the two vacancies, of the Schottky defect in MgO. Values are shown for (a) Mg and (b) O vacancies.

that the migration through a 3nn configuration [Fig. 5(b)] is associated with the lowest migration energies, 1.77 eV and 1.95 eV. Another possible transition starting from the 1nn configuration corresponds to a path through a 2nn configuration. This involves two energy barriers of 2.07 eV (V_{Mg} jump) and 2.29 eV (V_O jump), respectively. Here again, the NEB calculations validate the energy barriers found by kART.

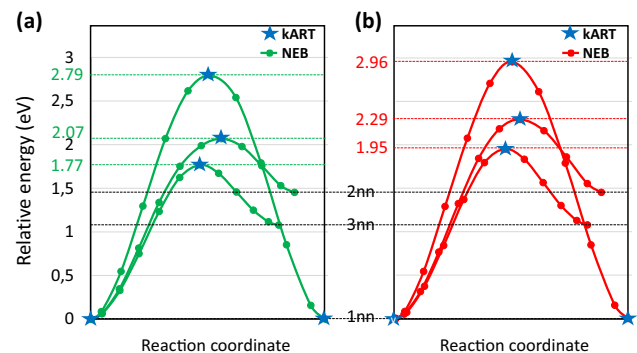


FIG. 7. Energy landscape of the three first mechanisms related to vacancy diffusion in the Schottky defect in MgO. The figure shows the energy barriers using NEB and kART calculations of vacancy jumps from first to first, second, and third nearest neighbor crystal position of (a) Mg and (b) O vacancies. The 2nn and 3nn are situated 1.45 and 1.08 eV above the 1nn state, respectively.

TABLE II. Migration energies of isolated vacancies in MgO. Our values are compared to others obtained using density functional theory (DFT), molecular dynamics (MD), and experimental (Exp) results. All values are in eV.

Migration energy	This work	Other works
Mg vacancy	1.53	1.82 [16] _{DFT} , 1.70 [12] _{MD} , 2.17 [38] _{Exp}
O vacancy	1.70	1.93 [16] _{DFT} , 1.97 [12] _{MD} , 2.43 [39] _{Exp}

IV. DISCUSSION

Considering the study of the formation energy of the SD, dealing with an ionic solid, we had to take into account the electrostatic effects in the calculations involving periodic systems. By taking the long-range periodic interactions into account, the interactions between the defect and its own periodic images can be corrected and thus the formation energy can be evaluated accurately. The formation energy was seen to be generally increasing with the separation between the two vacancies except for the case of few exceptions as indicated in Table I. This can be explained by the ionic displacements involved during relaxation. Whereas the displacements of ions follow the trend of isolated vacancies, with cations and anions respectively attracted and repelled by V_{Mg} and the opposite for V_O , the magnitudes of displacements in the vicinity of the three nearest neighbor configurations are larger and lead to a nonmonotonic evolution of the formation energy with the distance d between the pair of vacancies. We observe that the three first nearest neighbor configurations are associated with significantly lower formation energies. Also, one may notice the higher stability of the 3nn configuration compared to 2nn. This result is in good qualitative agreement with DFT calculations. In particular, the evolution of the formation energy as a function of the separation distance of the vacancies is well reproduced with the configuration involving isolated vacancies being the most energetic. It is worth noting that the parametrization of the potential used here allows for formation energies in the range of those determined from DFT considering the different approximation LDA [13] and GGA [16,34]. As shown Table I, the Ball and Grimes potential systematically overestimates the DFT-GGA results and underestimates the LDA formation energies by less than 0.5 eV.

Similarly, the migration energies are slightly underestimated compared to the DFT barriers available (Table II). Nevertheless, the migration energy barriers found when vacancies move as isolated defects show a faster diffusion of the cationic vacancies (1.53 eV for Mg vacancies to compare with 1.70 eV for O vacancies) in agreement with all previous studies [11–13,16]. When sufficiently distant, the migration energy barriers of both vacancies are lower than those in nearer configurations which implies a faster diffusion as observed in the transient regime, before aggregation (Fig. 4). Such a behavior is again consistent with some DFT calculations showing that the migration energy for a divacancy (taken as the maximum of the two barriers for magnesium and oxygen hops) is higher than the ones of the isolated Schottky defect.

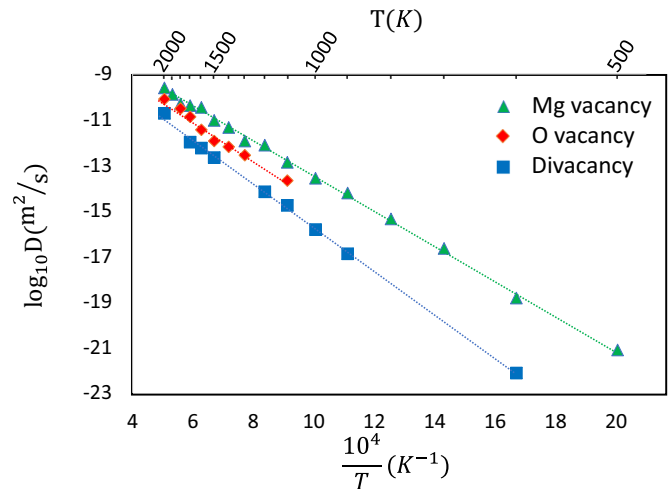


FIG. 8. Diffusion coefficient of individual vacancies and Schottky defects in MgO extracted from MSD plots. Green triangles, red diamonds, and blue squares refer to Mg monovacancy, O monovacancy, and divacancy, respectively.

The MSD plots presented in Fig. 4 allow us to calculate the diffusion coefficient of the migrating species according to $\frac{\langle D^2 \rangle}{\beta t}$ where $\langle D^2 \rangle$ is the mean squared displacement, β is a coefficient which depends on the dimensionality of the system and on the number of accessible jumps (here we took $\beta = 6$), and t is time. The values obtained by kART are plotted in Fig. 8.

Our calculations provide a detailed description of the mechanisms at play during diffusion with the MSD clearly exhibiting two regimes separated by a change of slope. The first regime corresponds to the transient state where the oxygen and the magnesium vacancy converge together until the minimum energy configuration is met. The pathways are illustrated in Fig. 6. At high temperature (i.e., above about 1200 K) both oxygen and magnesium vacancy jumps contribute to the evolution. This stage allows us to derive values for calculating diffusion coefficients of Mg and O vacancies which are reported on Fig. 8. All the selected events are shown depending on their energy barrier height in Fig. 9. This figure shows the different events corresponding to dissociation or/and aggregation between the vacancies. Below 1200 K, V_O jumps become less frequent and aggregation eventually occurs in our cell through V_{Mg} jumps only, before any V_O occurs. This is well illustrated by the compilation of all events shown in Fig. 9(a). In this regime and in this temperature range, we can only determine the diffusion coefficient of V_{Mg} . This is why Fig. 8 displays values for V_{Mg} in the whole temperature range while for V_O , only values at high temperatures are accessible. Diffusion of Mg vacancies is faster with an activation energy of 1.53 eV. Diffusion of O vacancies is slower and exhibits a larger activation energy of 1.70 eV. These values are in excellent agreement with the energy barriers described above.

A major output of our work is to describe the evolution of the divacancy (i.e., the bound SD) and its dynamics. Figure 8 shows that global displacements of the bound SD defects have occurred in the whole temperature range allowing us

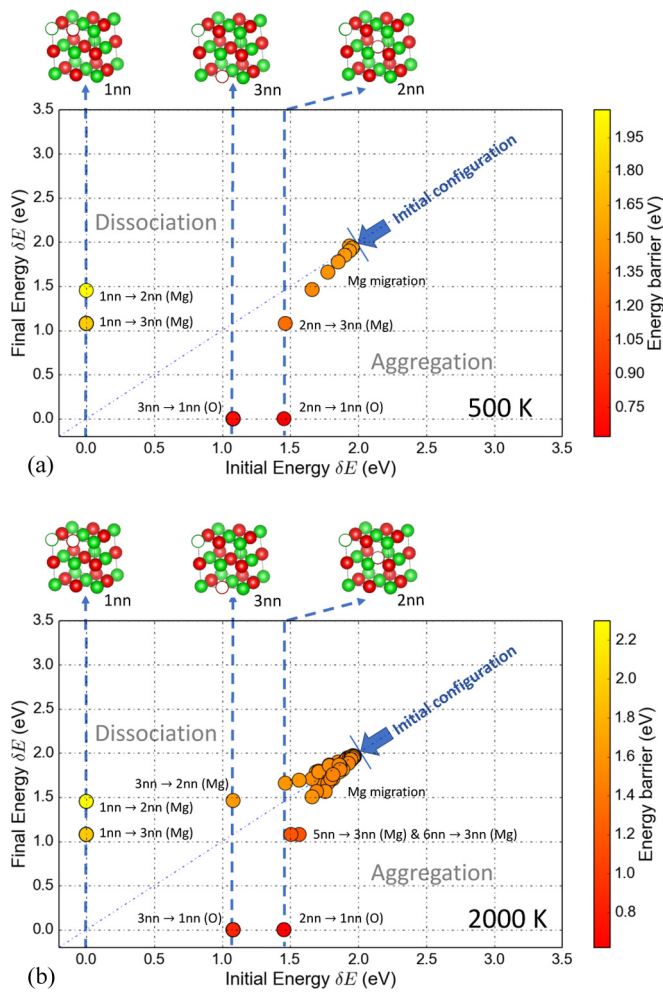


FIG. 9. Representation of all the accepted activation events for the Schottky defects in MgO starting from far vacancies until aggregation and further events involved in the calculation of the diffusion coefficient of the divacancy at (a) 500 K and (b) 2000 K. Energy barriers of each event are indicated with the color bar on the right of the figure. The most significant events are labeled. The configurations of the three most stable states (1nn, 2nn, and 3nn) are represented above the graph. The green and red spheres represent Mg and O atoms, respectively. The empty spheres refer to vacancies. The upper part of the graph corresponds to “dissociation,” i.e., to events which tend to separate vacancies. Reciprocally, “aggregation,” in the lower part, refers to events which bring vacancies together leading eventually to the lowest energy configurations. All initial and final energies are evaluated with respect to 1nn, considered as the ground state, and set to 0. All values are in eV.

to determine the evolution of its diffusion coefficient from 2000 K down to 500 K.

Here again, it is relevant to discuss separately the behaviors at “low” and “high” temperatures. Below 1200 K, once aggregation is achieved, the divacancy is very stable. Figures 9(a) and 10 show that only transitions between 1nn and 3nn occur. In most cases, after the 3nn is reached through a V_{Mg} jump over a 1.77 eV barrier, it is rapidly followed by a back jump since the corresponding energy barrier is only 0.69 eV. However, in some cases the transition from 3nn to 1nn occurs through a V_O jump over a 0.87 eV barrier. This succession

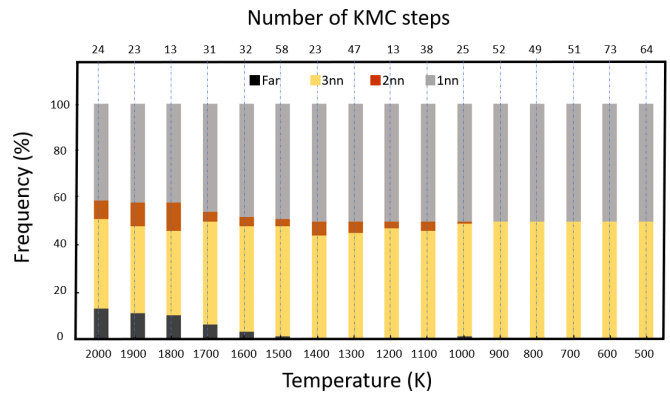


FIG. 10. Histogram showing the frequency of visited states (1nn, 2nn, 3nn, and farther) depending on the simulation temperature (in the range 500–2000 K with steps of 100 K). The number of simulation steps is shown in the top of the figure. The count is started when the dominant change in the slope in the MSD is spotted (Fig. 8).

of events corresponds to a net jump of the divacancy. The behavior at high temperature is slightly more complex since under thermal activation, more configurations are explored as shown by Figs. 10 and 9(b). In particular, 2nn configurations are sometimes reached. However, Fig. 8 shows that the global kinetics is not affected and that the net displacement of the divacancy is still constrained by the same barriers. Overall, the diffusion of the aggregated defect is slower than V_O diffusion since it requires correlated V_O and V_{Mg} jumps. The resulting activation energy is 1.91 ± 0.05 eV which lies in between 1.77 and 1.95 eV, i.e., the two barriers describing jumps of V_O and V_{Mg} between the 1nn and the 3nn configurations.

V. CONCLUSION

Using the kART method, we provide the first complete description of the energy landscape for the migration of bound Schottky defects in MgO. Initially, the reliability of the potential was checked by comparing the obtained formation energies of different configurations to available *ab initio* and experimental values. We suggest taking into consideration two types of corrections when calculating the formation energy of such defects in ionic crystals. Our results are in good agreement with literature values concerning formation energies. Then, we report a preferred recombination of vacancies to form the aggregated Schottky defect. Before aggregation, we have studied the evolution of the energy barriers as the individual vacancies become closer. As expected, our results show a faster diffusion of cationic compared to anionic vacancies. In the aggregated Schottky defect configuration, we have demonstrated an unexpected richness of the kinetics that governs its movement involving different possible transient configurations (e.g., 2nn or 3nn). We have also calculated the diffusion coefficients at different temperatures. The kART method allows us to investigate diffusion at very low temperatures which are unreachable by experiment and classical simulation methods. After aggregation, the easiest diffusion path of the defect was identified in detail by giving the values of energy barriers at each step of the mechanism. This

latter is a two-step process characterized by a succession of a cationic vacancy jump followed by the anionic vacancy jump. In addition, some less favorable mechanisms of Schottky defect diffusion are identified which are only activated at high temperature.

ACKNOWLEDGMENTS

This project has received funding from the European Research Council (ERC) under the European Union's Horizon 2020 research and innovation program under Grant Agreement No. 787198, TimeMan.

-
- [1] P. A. Burr and M. W. D. Cooper, Importance of elastic finite-size effects: Neutral defects in ionic compounds, *Phys. Rev. B* **96**, 094107 (2017).
- [2] C. Zhang, X. Wang, J. Zhang, K. Yang, Y. Cheng, Z. Zeng, X. Zhou, and H. Lin, Schottky defects induced effects on the behaviors of high velocity shock compression of MgO, *RSC Adv.* **7**, 45304 (2017).
- [3] D. Singh, N. Singh, S. K. Gupta, and Y. Sonvane, Effect on electronic and optical properties of Frenkel and Schottky defects in HfS₂ monolayer, in *DAE Solid State Physics Symposium 2017*, AIP Conf. Proc. No. 1942 (AIP, New York, 2018), p. 090023.
- [4] F. El-Mellouhi, N. Mousseau, and L. J. Lewis, Kinetic activation-relaxation technique: An off-lattice self-learning kinetic Monte Carlo algorithm, *Phys. Rev. B* **78**, 153202 (2008).
- [5] N. Mousseau, L. K. Béland, P. Brommer, F. El-Mellouhi, J. F. Joly, G. K. N'tsouaglo, O. A. Restrepo, and M. Trochet, Following atomistic kinetics on experimental timescales with the kinetic activation relaxation technique, *Comput. Mater. Sci.* **100**, 111 (2015).
- [6] S. Mahmoud, M. Trochet, O. A. Restrepo, and N. Mousseau, Study of point defects diffusion in nickel using kinetic activation-relaxation technique, *Acta Mater.* **144**, 679 (2018).
- [7] S. Mahmoud and N. Mousseau, Long-time point defect diffusion in ordered nickel-based binary alloys: How small kinetic differences can lead to completely long-time structural evolution, *Materialia* **4**, 575 (2018).
- [8] J. Goniakowski and C. Noguera, Insulating oxide surfaces and nanostructures, *C. R. Phys.* **17**, 471 (2016).
- [9] I. O. Wilson, Magnesium oxide as a high-temperature insulant, *IEE Proc.-A: Sci., Meas. Technol.* **128**, 159 (1981).
- [10] M. H. Yang and C. P. Flynn, Intrinsic Diffusion Properties of an Oxide: MgO, *Phys. Rev. Lett.* **73**, 1809 (1994).
- [11] M. J. L. Sangster and D. K. Rowell, Calculation of defect energies and volumes in some oxides, *Philos. Mag. A* **44**, 613 (1981).
- [12] J. Ita and R. E. Cohen, Effects of Pressure on Diffusion and Vacancy Formation in MgO from Nonempirical Free-Energy Integrations, *Phys. Rev. Lett.* **79**, 3198 (1997).
- [13] C. A. Gilbert, S. D. Kenny, R. Smith, and E. Sanville, *Ab initio* study of point defects in magnesium oxide, *Phys. Rev. B* **76**, 184103 (2007).
- [14] A. De Vita, M. J. Gillan, J. S. Lin, M. C. Payne, I. Stich, and L. J. Clarke, Defect Energetics in Oxide Materials from First Principles, *Phys. Rev. Lett.* **68**, 3319 (1992).
- [15] B. P. Uberuaga, R. Smith, A. R. Cleave, G. Henkelman, R. W. Grimes, A. F. Voter, and K. E. Sickafus, Dynamical simulations of radiation damage and defect mobility in MgO, *Phys. Rev. B* **71**, 104102 (2005).
- [16] M. W. Ammann, J. P. Brodholt, and D. P. Dobson, Simulating diffusion, *Rev. Mineral. Geochem.* **71**, 201 (2010).
- [17] M. W. Ammann, Diffusion in minerals of the Earth's lower mantle: Constraining rheology from first principles, Ph.D. thesis, University College London, 2011.
- [18] S. Plimpton, Fast parallel algorithms for short-range molecular dynamics, *J. Comput. Phys.* **117**, 1 (1995).
- [19] R. J. Sadus, Particle-particle and particle-mesh (PPPM) methods, in *Molecular Simulation of Fluids: Theory, Algorithms and Object-Oriented* (Elsevier, Amsterdam, 1999), pp. 162–169.
- [20] G. Henkelman, B. P. Uberuaga, D. J. Harris, J. H. Harding, and N. L. Allan, MgO addimer diffusion on MgO(100): A comparison of *ab initio* and empirical models, *Phys. Rev. B* **72**, 115437 (2005).
- [21] E. Bitzek, P. Koskinen, F. Gähler, M. Moseler, and P. Gumbsch, Structural Relaxation Made Simple, *Phys. Rev. Lett.* **97**, 170201 (2006).
- [22] A. Cimino, P. Porta, and M. Valigi, Dependence of the lattice parameter of magnesium oxide on crystallite size, *J. Am. Ceram. Soc.* **49**, 152 (1966).
- [23] M. Kiguchi, S. Entani, K. Saiki, T. Goto, and A. Koma, Atomic and electronic structure of an unreconstructed polar MgO(111) thin film on Ag(111), *Phys. Rev. B* **68**, 115402 (2003).
- [24] L. K. Béland, P. Brommer, F. El-Mellouhi, J.-F. Joly, and N. Mousseau, Kinetic activation-relaxation technique, *Phys. Rev. E* **84**, 046704 (2011).
- [25] M. Trochet, A. Sauvé-Lacoursière, and N. Mousseau, Algorithmic developments of the kinetic activation-relaxation technique: Accessing long-time kinetics of larger and more complex systems, *J. Chem. Phys.* **147**, 152712 (2017).
- [26] B. D. McKay *et al.*, Practical graph isomorphism, *Congressus Numerantium* **30**, 45 (1981).
- [27] G. T. Barkema and N. Mousseau, Event-Based Relaxation of Continuous Disordered Systems, *Phys. Rev. Lett.* **77**, 4358 (1996).
- [28] R. Malek and N. Mousseau, Dynamics of Lennard-Jones clusters: A characterization of the activation-relaxation technique, *Phys. Rev. E* **62**, 7723 (2000).
- [29] M.-C. Marinica, F. Willaime, and N. Mousseau, Energy landscape of small clusters of self-interstitial dumbbells in iron, *Phys. Rev. B* **83**, 094119 (2011).
- [30] K. J. Laidler and M. C. King, Development of transition-state theory, *J. Phys. Chem.* **87**, 2657 (1983).
- [31] L. Le Cam, An approximation theorem for the Poisson binomial distribution, *Pacific J. Math.* **10**, 1181 (1960).
- [32] G. Henkelman, B. P. Uberuaga, and H. Jónsson, A climbing image nudged elastic band method for finding saddle points and minimum energy paths, *J. Chem. Phys.* **113**, 9901 (2000).
- [33] G. Henkelman and H. Jónsson, Improved tangent estimate in the nudged elastic band method for finding minimum energy paths and saddle points, *J. Chem. Phys.* **113**, 9978 (2000).

- [34] O. Runevall and N. Sandberg, Self-diffusion in MgO: A density functional study, *J. Phys.: Condens. Matter* **23**, 345402 (2011).
- [35] D. Alfè and M. J. Gillan, Schottky defect formation energy in MgO calculated by diffusion Monte Carlo, *Phys. Rev. B* **71**, 220101(R) (2005).
- [36] M. Leslie and N. J. Gillan, The energy and elastic dipole tensor of defects in ionic crystals calculated by the supercell method, *J. Phys. C* **18**, 973 (1985).
- [37] A. Jay, C. Huet, N. Salles, M. Gunde, L. Martin-Samos, N. Richard, G. Landa, V. Goiffon, S. De Gironcoli, A. Hémerlyck, and N. Mousseau, Finding reaction pathways and transition states: r-ARTn and d-ARTn as an efficient and versatile alternative to string approaches, *J. Chem. Theory Comput.* **16**, 6726 (2020).
- [38] S. Mackwell, M. Bystricky, and C. Sproni, Fe-Mg interdiffusion in (Mg,Fe)O, *Phys. Chem. Miner.* **32**, 418 (2005).
- [39] S. Shirasaki and M. Hama, Oxygen-diffusion characteristics of loosely-sintered polycrystalline MgO, *Chem. Phys. Lett.* **20**, 361 (1973).